JOURNAL OF SOLID STATE CHEMISTRY **139,** 45–51 (1998)
ARTICLE NO. SC987799

$AuTa_5S$: A Cubic Rod Packing of Condensed $(Au, Ta)_{13}$ Icosahedra Interwoven with a Three-Dimensional Framework of Corner-Connected STa_6 Octahedra

Bernd Harbrecht, Volker Wagner, and Clemens Pietzonka

Fachbereich Chemie and Center for Material Sciences, Philipps-Universitaet, D-32043 Marburg, Germany

Received July 17, 1997; accepted February 26, 1998

$AuTa_5S$ was prepared from a compressed mixture of tantalum disulfide, tantalum, and gold in a sealed tantalum capsule at 1650 K within 2 days. Above 1750 K the sulfide disproportionates in the solid state. The structure of $AuTa_5S$ ($a = 1250.82(3)$ pm, $F\bar{4}3m$, $Z = 16$, Pearson symbol $cF112$) was determined from integrated X-ray powder diffraction intensities by direct methods and subsequently refined by fitting the profiles (13 structure variables, $R_{wp} = 0.036$). Three of five crystallographically distinct metal atoms have distorted icosahedral coordinations. Sulfur is trigonal antiprismatically coordinated by tantalum. The structure is composed of two mutually interpenetrating zinc blende-like frameworks consisting of corner-connected STa_6 octahedra and corner-connected Au_4Ta_4 and Ta_4Ta_4 stellae quadrangulae. The unique structure of $AuTa_5S$ represents a link between two major intermetallic structure families, the η-carbide-type and the $Mn_{23}Th_6$-type structures.

INTRODUCTION

Icosahedral coordination is a dominant structural feature of hundreds of intermetallic phases. Prominent representatives are the Frank–Kasper phases (1–3), many of which consist of transition metals or additionally contain aluminum or silicon as a main-group element. However, there are also a small number of phases among metal-rich pnictides and chalcogenides forming structures composed of metal-centered M_{13} icosahedra, e.g., $Pd_{15}P_2$ (4) and several tantalum-rich sulfides (5–10).

The first representatives of the sulfides, Ta_2S (5) and Ta_6S (6), were found by Franzen and Smeggil more than two decades ago. A triclinic modification of Ta_6S (7) and the $n = 4$ member of a Ta_6S_n series (8–10) were characterized more recently. Thermodynamic data (11) and electronic transport properties (12) have also been reported for the sulfides. In addition, we have shown that increased substitution of vanadium for chromium for tantalum in Ta_6S triggers a displacive phase transition (13). Other chalcogenides such as Ta_6Te_5 (14) and $Ta_5(Se, Te)_3$ (15) and the intermetallic phase τ-$Al_{2.9}Ta_{2.7}V_{1.4}$ (16) were found to form related structures.

In view of the possibility of structurally modifying the tantalum-rich sulfides by partial substitution of tantalum, we investigated preparatively selected ternary systems in the tantalum-rich regions. As a third minor component we chose metals which form Frank–Kasper phases with tantalum. We assumed that such metals might stabilize icosahedral coordination in tenary metal-rich chalcogenides. Indeed, in the ternary system Au–Ta–S, we uncovered two new tantalum-rich phases: $Au_xTa_{15-x}S_2$ ($x = 0.3$–1.1) (17), being isotypic with $Pd_{15}P_2$ and adopting a stuffed α-boron-related structure, and a metal-rich 6 : 1 sulfide, the structure of which differs completely from those of other $(Ta, M)_6S$ compounds. The structure of $AuTa_5S$ represents a derivative of the η-carbide structure type and can also be viewed as a defect variant of the $Mn_{23}Th_6$ (18) structure type. The synthesis and structure of this ternary sulfide are the subject of this report.

EXPERIMENTAL

Sample Preparation and Phase Analyses

$AuTa_5S$ was prepared from an appropriate, compressed mixture of $Ta_{1.3}S_2$ (19) and the metals (about 500 mg; Ta: 99.98%, Ventron; Au: 99.99%, Degussa; S: DAB6, Merck) in a sealed tantalum tube in a vaccum ($P < 0.01$ Pa) at 1650 K within 2 days. Loss of sulfur due to reaction with the container wall was taken into account by using an excess of sulfur in the starting mixture. The composition of the phase was delimited preparatively by systematic variation of the ratio of the elemental components Au : Ta : S from 0.5 : 5 : 0.7 to 2 : 5 : 2.

Semiquantitative energy-dispersive analyses of emitted X-rays (EDX, PV 9800, Edax) of sphere like crystals (ca. 3 μm) in a scanning electron microscope (SEM, DMS 940, Zeiss) yielded $Au_{1.0(1)}Ta_{5.0(3)}S_{1.1(1)}$.

The samples were examined by X-ray powder diffraction with use of a Guinier camera ($CuK\alpha_1$, Enraf-Nonius) and/or

0022-4596/98 $25.00

a diffractometer (Cu$K\alpha$, PW1050/25, Philips). The cubic lattice parameter of $AuTa_5S$ was found to vary between 1250.7(1) and 1251.36(8) pm. Opposed to the findings for $Au_xTa_{15-x}S_2$ (17), there are no indications for a marked homogeneity range. The fcc lattice was confirmed by electron diffraction (EM 300, Philips) along four- and threefold zone axes.

$AuTa_5S$ starts to form at 1500 K and presists up to about 1750 K. Above 1750 K it decomposes in the solid state, yielding $Au_xTa_{15-x}S_2$ (17), tetragonal $Au_{1-x}Ta_x$ ($x \approx 0.5$) (20), and a $2H$-$Ta_{1+x}S_2$-type phase. Samples richer in gold than $AuTa_5S$ additionally contained σ-$AuTa_2$ (20) or $Au_{1-x}Ta_x$. In sulfur-rich samples a $2H$-$Ta_{1.3}S_2$-type phase (19) and Ta_2S (5) or Ta_3S_2 (8,9) were identified as byproducts. Sulfur deficient samples contained a bcc-type solid solution and/or $Au_xTa_{15-x}S_2$ as byproducts.

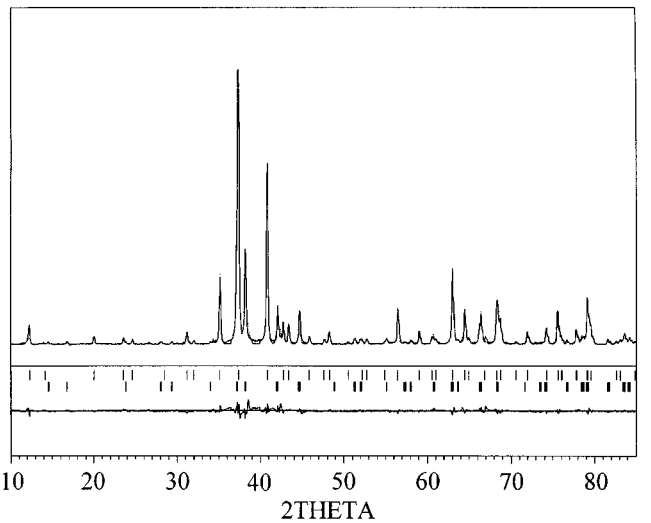

FIG. 1. X-ray powder diffractogram (Cu$K\alpha$) of $AuTa_5S$ containing $AuTa_{14}S_2$ as a minor component. The difference between the measured and calculated diffractogram is shown at the bottom of the lower panel. The upper part of this panel shows the Bragg angles for $AuTa_5S$ (first row) and $AuTa_{14}S_2$ (second row).

Structure Determination

All attempts to grow crystals of a suitable size for an X-ray structure determination failed. Therefore the structure was solved from X-ray powder diffraction intensities measured in the range $10^\circ < 2\theta < 100^\circ$ in a step width of 0.03°, each point for 45 s. Deconvolution and integration of the intensities were done with the local program DIFFRAKT (21). The raw intensities were corrected by the Lorentz–polarization and the multiplicity factors. Structure calculations were performed with the programs SHELXS86 (22) and SHELXL93 (23). The final Rietveld profile fitting was done with the program LHPM (24).

The observed extinctions were compatible with the symmorphic space group types $Fm3m$, $F\bar{4}3m$, $F432$, $Fm\bar{3}$, and $F2\bar{3}$. A further reduction of the space groups was possible assuming an ordered structure of composition $AuTa_5S$ with 16 formula units per cell. These restraints require a 16-fold site in addition to the high-symmetry sites, leading to the noncentrosymmetric space groups $F2\bar{3}$ and $F\bar{4}3m$, of which the high-symmetry groups turned out to be correct. The solution of the structure by direct methods was attempted with 25 symmetrically independent intensities. Thirty-six additional intensities were omitted on account of perfect superposition of at least two symmetrically independent intensities. In spite of the restricted number of intensities, two metal sites, $16e(x, x, x)$ ($x = 0.38$) and $24f(x, 0, 0)$ ($x = 0.20$), could be extracted from the proposed structure models. Subsequent difference Fourier syntheses using 42 intensities revealed the remaining four sites, including that of the sulfur atom. The calculations converged at $R(F) = 0.043$, $R_w(F^2) = 0.143$. The residual charge density at possible interstitial sites such as $4a$, $4b$, and $4d$ was shown to be negligible. The structure was confirmed by fitting the X-ray intensity profiles ($R_{wp} = 0.036$, $R_I = 0.014$) of a sample containing $Au_xTa_{15-x}S_2$ as a minor component. The profile fit is shown in Fig. 1. Relevant parameters of the Rietveld refinement are listed in Table 1. Table 2 contains the indices, the d-values, and the calculated and observed intensities for $AuTa_5S$. The positional and isotropic displacement parameters and selected interatomic distances are listed in Tables 3 and 4, respectively.

TABLE 1
Rietveld Refinement Parameters for $AuTa_5S$

Technical data	
2θ range (deg)	10–100
Step size (deg)	0.03
Time per step (s)	45
X-ray	Cu$K\alpha$
Global parameters	
Number of phases	2
Number of variables	45
Profile fit	Pseudo-Voigt
Background	Refined
Structural and profile data	
Molar mass (g mol^{-1})	1133.8
Space group (No.)	$F\bar{4}3m$(216)
Lattice parameter a (pm)	1250.82(3)
Formula units per unit cell	16
Density ρ_x (g cm^{-3})	15.39
FWHM Parameters u, v, w	0.11(1), $-$0.11(1), 0.055(3)
Asymmetry parameter	0.80(4)
Profile parameter γ	0.66(2)
R_p, R_{wp}	0.025, 0.036
$R_I(AuTa_5S)$, $R_I(AuTa_{14}S_2)$	0.014, 0.011

TABLE 2
Indices, *d*-Values, and Observed and Calculated Intensities for $AuTa_5S$

hkl	*d*	I_{obs}	I_{calc}
111	7.2214	91	94
220	4.4224	34	35
311	3.7713	23	23
222	3.6108	18	17
331	2.8695	45	48
420	2.7969	15	15
422	2.5532	309	305
511/333	2.4072	1000	752/245
440	2.2111	843	834
531	2.1143	78	79
442/600	2.0847	88	84/3
620	1.9777	34	34
533	1.9075	17	17
622	1.8857	54	53
444	1.8054	9	10
551/711	1.7516	13	5/9
640	1.7346	21	21
642	1.6715	6	6
553/731	1.6284	168	58/114
800	1.5635	58	60
733	1.5281	29	28
820/644	1.5168	15	1/14
660/822	1.4741	266	116/157
751/555	1.4443	170	22/148
662	1.4348	25	24
753/911	1.3729	68	38/31
842	1.3648	99	101
664	1.3334	10	10
931	1.3112	60	61
844	1.2766	69	71
933/771/755	1.2571	179	106/51/24
1000/860	1.2508	35	8/27
1020/862	1.2265	78	33/45
951/773	1.2092	221	143/81
1022/666	1.2036	75	55/21
953	1.1664	16	16
864/1040	1.1614	22	9/13
1042	1.1418	16	16
775/1111	1.1278	14	12/3
880	1.1056	23	23
955/1131/971	1.0928	64	40/14/10
1044/882	1.0887	49	13/34

STRUCTURE DESCRIPTION AND DISCUSSION

$AuTa_5S$ represents a new structure type of cubic symmetry with 112 atoms per unit cell. The structure is built up by six crystallographically inequivalent atoms, Au(1), Ta(1) to Ta(4), and S(1). The distinct coordination polyhedra are shown in Fig. 2. Fifty percent of the atoms have distorted icosahedral coordinations. Au(1) and Ta(1) are surrounded exclusively by 12 metal atoms. The scattering of the distances between (i) the central and the peripheral atoms (d_{c-p}), (ii) between all pairs of the peripheral atoms (d_{p-p}), and (iii) the ratio of the mean distances $\langle d_{c-p}\rangle/\langle d_{p-p}\rangle$ reflects the deviation from icosahedral coordination. The values for Au(1) are $\langle d_{c-p}\rangle = 290.0$ pm (284.3–300.5 pm) and $\langle d_{p-p}\rangle = 305.6$ pm (284.3–310.7 pm) and those for Ta(1) are $\langle d_{c-p}\rangle = 292.1$ pm (274.2–310.7 pm) and $\langle d_{p-p}\rangle = 305.4$ pm (277.0–360.2 pm). In spite of a larger scattering of Ta(1)–*M* distances than of Au(1)–*M* distances, the ratios $\langle d_{c-p}\rangle/\langle d_{p-p}\rangle$ (0.949 and 0.953, respectively) of both configurations are close to the value of an icosahedron $(\frac{1}{2}[1 + 2\cos 2\pi/5)^2]^{1/2} = 0.951)$. Ta(3) also has the coordination number (CN) 12. However, two neighboring S(1) (244 pm) give rise to a strong distortion of the icosahedron: $\langle d_{c-p}\rangle = 291.8$ pm (244–321.7 pm), $\langle d_{p-p}\rangle = 304.5$ pm (248–349.4 pm), and $\langle d_{c-p}\rangle/\langle d_{p-p}\rangle = 0.958$. Ta(2) with CN 16 has a pentagonal prismatic coordination with six additional atoms. Two Au(1) cap the pentagonal faces; two S(1) and two Ta(4) are situated above four rectangular faces. The fifth face is common to two Ta(2) coordination polyhedra, which share an empty $Ta(2)_6$ octahedron (349.4 pm) situated around a point of high symmetry ($\bar{4}3m$, Wyckoff position 4*d*). The coordination polyhedron about Ta(4) is a tricapped

TABLE 3
Positional and Isotropic Displacement Parameters (10^4 pm^2) for $AuTa_5S$

Atom	Site	*x*	*y*	*z*	*B*
Au(1)	16*e*	0.1687(3)	0.1687	0.1687	0.6(1)
Ta(1)	16*e*	0.3836(5)	0.3836	0.3836	0.6(2)
Ta(2)	24*f*	0.1975(5)	0	0	1.1(1)
Ta(3)	24*g*	0.9698(5)	0.25	0.25	1.2(2)
Ta(4)	16*e*	0.6018(3)	0.6018	0.6018	0.7(1)
S(1)	16*e*	0.8676(15)	0.8676	0.8676	1(1)

TABLE 4
Characteristic Interatomic Distances (pm) for $AuTa_5S$

Au(1)–3 × Ta(1)	284.3(7)	Ta(3)–2 × S(1)	244(2)
–3 × Ta(3)	287.4(4)	–2 × Ta(4)	277.0(4)
–3 × Au(1)	287.7(5)	–2 × Au(1)	287.4(6)
–3 × Ta(2)	300.5(6)	–2 × Ta(1)	299.1(7)
–3 × S(1)	382(2)	–4 × Ta(2)	321.7(1)
		–4 × Ta(3)	388.8(6)
Ta(1)–3 × Ta(4)	274.2(7)	Ta(4)–3 × Ta(1)	274.2(7)
–3 × Au(1)	284.3(7)	–3 × Ta(3)	277.0(5)
–3 × Ta(3)	299.1(7)	–3 × Ta(2)	308.9(5)
–3 × Ta(2)	310.7(6)	–3 × S(1)	337(2)
–3 × Ta(1)	411.8(8)	–3 × Ta(4)	360.2(5)
Ta(2)–2 × S(1)	248(2)	S(1)–3 × Ta(3)	244(2)
–2 × Au(1)	300.5(4)	–3 × Ta(2)	248(2)
–2 × Ta(4)	308.9(6)	–3 × Ta(4)	337(2)
–2 × Ta(1)	310.7(7)	–3 × Au(1)	382(2)
–4 × Ta(3)	321.7(2)		
–4 × Ta(2)	349.4(6)		
–2 × S(1)	475(2)		

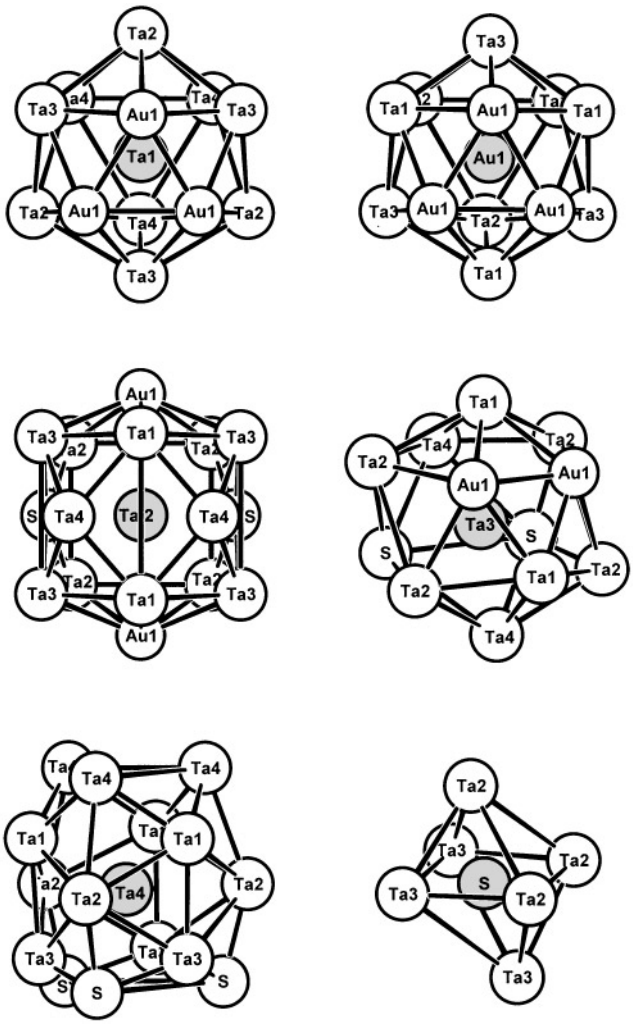

FIG. 2. Coordination polyhedra about all six crystallographically distinct atoms of $AuTa_5S$.

trigonal prism ($\langle d_{Ta(4)-Ta}\rangle = 286.7$ pm) with three S(1) and three Ta(4) above each of the trigonal faces, respectively. S(1) is trigonal antiprismatically surrounded by three Ta(2) and three Ta(3) ($\langle d_{Ta-Ta}\rangle = 345.4$ pm, $\langle d_{S-Ta}\rangle = 246$ pm).

Four of the five crystallographically distinct metal atoms form 26 atom clusters as present in γ-brass (25) and related phases (26). Each cluster consists of four shells: Four Au(1) form an inner tetrahedron (IT) ($d_{Au(1)-Au(1)} = 287.7$ pm) around high-symmetry points at, e.g., $(\frac{1}{4}, \frac{1}{4}, \frac{1}{4})$. Ta(1), situated above the faces of an $Au(1)_4$ tetrahedron, builds up an outer tetrahedron (OT) ($d_{Ta(1)-Ta(1)} = 411.8$ pm). Above the edges of the inner tetrahedron of this so-called stella quadrangula (27), which is composed of a central tetrahedron ($Au(1)_4$) and four capping tetrahedra ($Au(1)_3Ta(1)_1$) sharing faces with the central one, there are six Ta(3) forming an octahedron (OH) ($d_{Ta(3)-Ta(3)} = 388.6$ pm). Twelve Ta(2) complement the 26-atom cluster. They compose a distorted cuboctahedron (CO) which is confined by six rectangular and four larger and four smaller triangular faces. The 26-atom clusters are organized according to the motif of a cubic close packing. Moreover, the clusters are connected to 12 adjacent clusters via common Ta(2). The remaining Ta(4) are located close to the centers of the larger triangular faces of the distorted $Ta(2)_{12}$ CO. This view of the metal substructure is illustrated in Fig. 3. Figure 4 shows a polyhedral drawing of the OH shell togehter with the specifically distorted CO shell representing the surface of a cluster which consists of four interpenetrating icosahedra about Au(1) with a common $Au(1)_4$ tetrahedron in the center.

A more instructive description of the structure makes use of the coordination polyhedra about two selected atoms: S(1) and Ta(1). Ta(1) is chosen because it has the other four distinct metal atoms in its primary coordination sphere. As seen from Fig. 5, Ta(1) icosahedra are connected via common $Ta(4)_2Ta(2)$ and $Au(1)_2Ta_3$ faces forming rods which run parallel to the six face diagonals of the unit cell. Three orthogonally extending, adjacent rods partly intersect around high-symmetry points ($\bar{4}3m$, site $4c$ $(\frac{1}{4}, \frac{1}{4}, \frac{1}{4})$). At these points four Ta(1) icosahedra are joined by common edges around a central $Au(1)_4$ tetrahedron. Such interpenetrating quadruples are arranged in a cubic close packed way. Owing to the deltahedral coordination of Au(1), Ta(1), and Ta(3), most of the metal atoms form tetrahedra. There are 12 distinct tetrahedra. A total of 456 tetrahedra fill 74.7% of the unit cell's space. Ta(2) and/or Ta(3) form distorted octahedra filling the rest of the space. Sixteen out of 24 octahedral sites per unit cell are occupied by sulfur atoms. The $Ta(2)_3Ta(3)_2S(1)$ octahedra are grouped tetrahedrally

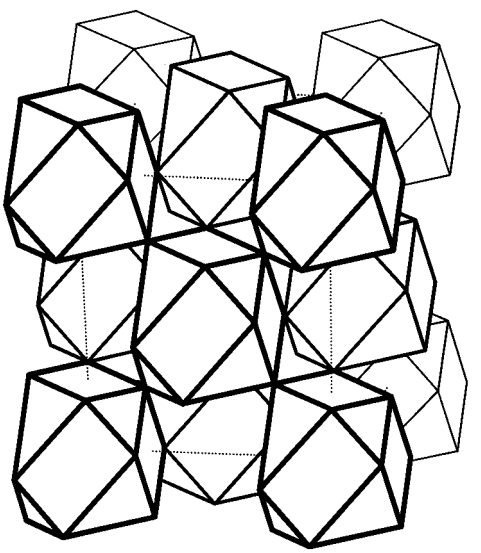

FIG. 3. Fcc arrangement of cuboctahedral shells of $Au(1)_4Ta(1)_4Ta(3)_6Ta(2)_{12}$ clusters as present in $AuTa_5S$. Note that the clusters are condensed via Ta(2) forming the distorted cuboctahedral shell.

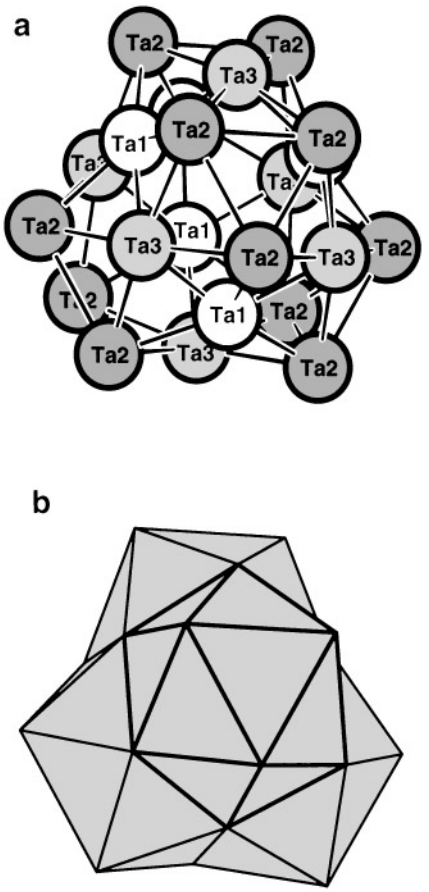

FIG. 4. (a) The 26-atom cluster corresponding to four fused $AuTa_{12}$ icosahedra about Au sharing a common central Au_4 tetrahedron. For the sake of clarity, the common, central $Au(1)_4$ tetrahedron is left out. (b) Polyhedral representation of the 26-atom cluster.

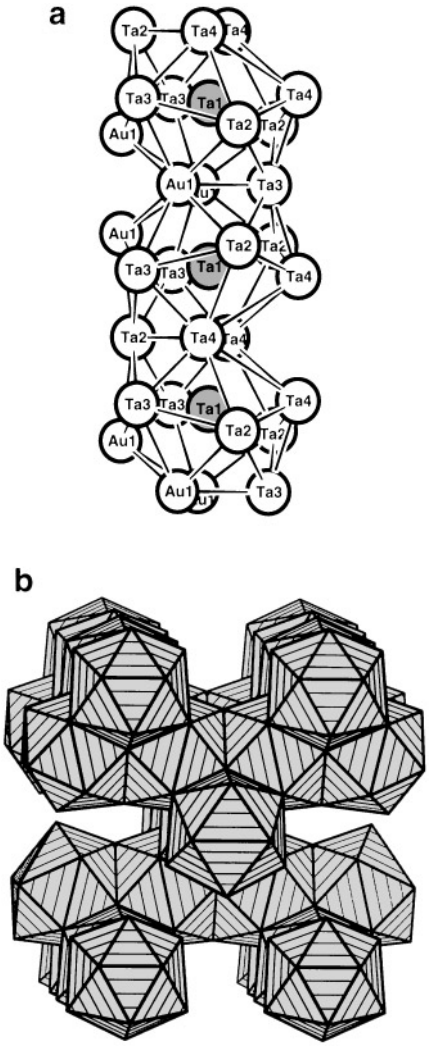

FIG. 5. (a) Three face-sharing $(Au, Ta)_{13}$ icosahedra about Ta(1) as part of an icosahedral rod extending parallel to all six face diagonals of the cubic unit cell. (b) Metal partial structure projected along [110] depicted as an icosahedral rod structure.

around the points of a diamond-like net. The points of the net are located in centers of empty octahedra, each of which is formed either by six Ta(2) around $4a(0,0,0)$ or by six Ta(3) around $4d(\frac{3}{4},\frac{3}{4},\frac{3}{4})$. Thus, the corner-sharing $^3_\infty[Ta_{6/2}S]$ octahedra are arranged like octahedral $^3_\infty[MO_{6/2}]$ groupings in pyrochlore-related structures (28). Figure 6 shows chains of tilted, corner-sharing $Ta_{6/2}S$ octahedra. They are connected by common Ta(2) and Ta(3) with chains of face-sharing icosahedra in planes lying parallel to the faces of the unit cell (see Fig. 5). From this point of view, the structure of $AuTa_5S$ arises from a mutual three-dimensional interpenetration of two independent frameworks, each filling the interstices of the other: a pyrochlore-like octahedral framework built up by Ta(2), Ta(3), and S(1) and a zinc blende-like framework of corner-connected stellae quadrangulae composed of Au(1), Ta(1), and Ta(4) (see Fig. 7). The specific orientation of the tetrahedral framework with respect to the octahedral one affords a metal substructure corresponding to the rod packing of face-sharing icosahedra about Ta(1) as shown in Fig. 5b.

Thus, the structure of $AuTa_5S$ represents a new intermetallic structure variant of a pyrochlore-related arrangement as found for, e.g., $Al_{13}Cr_4Si_4$ ($F\bar{4}3m$, $cF84$) or $NiTi_2$ ($Fd\bar{3}m$, $cF96$) (29). The correlations between occupied point positions for CFe_3W_3 (η-carbide) ($Fd\bar{3}m$, $cF112$) (30) and $Mn_{23}Th_6$ ($Fm\bar{3}m$, $cF116$) (18) are explicitly given in Table 5. Accordingly, the structure of $AuTa_5S$ can be considered a low-symmetry variant of the η-carbide structure. Moreover, the correlations also reveal a symmetry relation existing between two important intermetallic structure families, the pyrochlore-related phases and the $Mn_{23}Th_6$-type structures. The structural relationship with the more symmetrical $Mn_{23}Th_6$ structure type is particularly instructive with regard to the partitioning of the 5*d* metals in the structure. There are two 32*f* sites in $Mn_{23}Th_6$, being

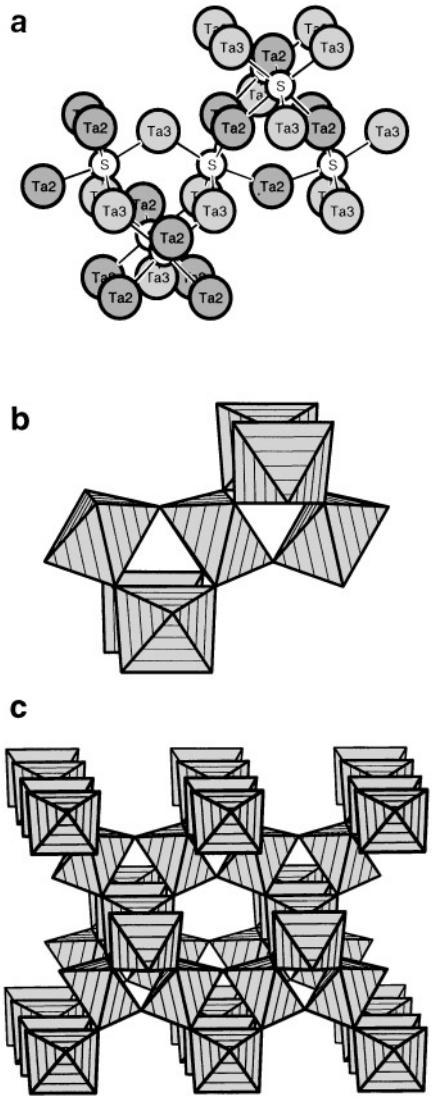

FIG. 6. (a) Ball-and-stick model and (b) polyhedral representation of two connected tetrahedrally arranged clusters consisting of four corner-connected TaS_6 octahedra about (0,0,0) and $(\frac{1}{4}, \frac{1}{4}, \frac{1}{4})$. (c) Three-dimensional zinc blende-like network of corner-sharing octahedra, $^3_\infty[Ta_{6/2}S]$ projected along [110].

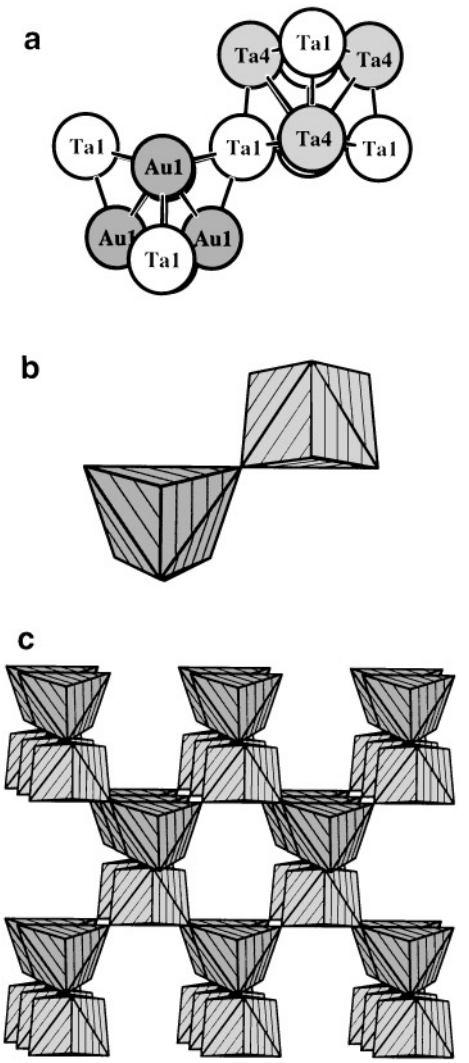

FIG. 7. (a) Ball-and-stick model and (b) polyhedral representation of vertex-sharing dodecahedral $Au(1)_4Ta(1)_4$ and $Ta(4)_4Ta(1)_4$ clusters, so-called stellae quadrangulae, each consisting of five fused tetrahedra. (b) Zinc blende-like network of corner-connected stellae quadrangulae which interpenetrates the porous octahedral pyrochlore-like network shown in Fig. 6c.

occupied by Mn(3) and Mn(4). In the low-symmetrical $AuTa_5S$ structure these two sites split into four 16*e* sites. One pair is occupied by Ta(1) and Ta(4), the other by the electronegative species, Au(1) and S(1), corresponding to the 32*f* Mn(4) site. Although gold diffracts Cu$K\alpha$ radiation only a little stronger than tantalum, there are two strong indications corroborating the given partition of the metal atoms in the structure: (i) The occupation of the 16*e* site ($x \approx \frac{1}{6}$) by Au leads to an unobtrusive displacement parameter, whereas the occupation of this site with Ta results in a suspiciously small displacement parameter ($B = 0.2 \times 10^4$ pm^2). (ii) Atoms on the 16*e* site ($x \approx \frac{1}{6}$) are exclusively coordinated by metal atoms as expected in this case for Au in view of the large difference between the affinities Ta–S (11) and Au–S (31).

CONCLUSIONS

(i) $AuTa_5S$ is accessible by application of high-temperature synthesis techniques. The tantalum-rich sulfide disproportionates in a peritectoid reaction above 1750 K.

(ii) The metal substructure of $AuTa_5S$ comprises icosahedral $(Au, Ta)_{13}$ clusters about Ta(1). The clusters are three-dimensionally condensed via common faces and edges

TABLE 5
Symmetry Relations between $AuTa_5S$, CFe_3W_3, and $Mn_{23}Th_6$

CFe_3W_3 (29) $Fd\bar{3}m$[a] $a = 1108.7$ pm		$AuTa_5S$ $F\bar{4}3m$ $a = 1250.8$ pm		$Mn_{23}Th_6$ (18) $Fm\bar{3}m$ $a = 1252.3$ pm
—		—		Mn(1), CN 14 $4b$ ($\frac{1}{2}, \frac{1}{2}, \frac{1}{2}$)
C(1), CN 6 $16c$ ($\frac{1}{8}, \frac{1}{8}, \frac{1}{8}$)	–	S(1), CN 6 $16e$ ($x = 0.8676$)		
			>	Mn(4), CN 12 $32f$ ($x = 0.1779$)
		Au(1), CN 12 $16e$ ($x = 0.1687$)		
Fe(2), CN 12 $32e$ ($x = 0.420$)	<			
		Ta(4), CN 16 $16e$ ($x = 0.6018$)		
			>	Mn(3), CN 13 $32f$ ($x = 0.3776$)
Fe(1), CN 12 $16d$ ($\frac{5}{8}, \frac{5}{8}, \frac{5}{8}$)	–	Ta(1), CN 12 $16e$ ($x = 0.3836$)		
		Ta(2), CN 16 $24f$ ($x = 0.1975$)	–	Th(1), CN 16 $24e$ ($x = 0.2047$)
W(1), CN 16 $48f$ ($x = 0.198$)	<			
		Ta(3), CN 12 $24g$ ($x = 0.9698$)	–	Mn(2), CN 12 $24d$ ($0, \frac{1}{4}, \frac{1}{4}$)

[a] Origin at $\bar{4}3m$.

along, e.g., [110] and [111] of the cubic unit cell, respectively. The sulfur atoms occupy two-thirds of all octahedral voids, resulting in a zinc blende-like network of corner-sharing STa_6 octahedra.

(iii) The unique structure of this tantalum-rich sulfide draws attention to a hitherto unnoticed structural relationship between $Mn_{23}Th_6$ and CFe_3W_3, the representatives of two major intermetallic structure families.

ACKNOWLEDGMENTS

Financial support by the Deutsche Forschungsgemeinschaft and the Fonds der Chemischen Industrie is gratefully acknowledged.

REFERENCES

1. F. C. Frank and J. S. Kasper, *Acta Crystallogr.* **11,** 184 (1958).
2. F. C. Frank and J. S. Kasper, *Acta Crystallogr.* **12,** 483 (1959).
3. D. P. Shoemaker and C. B. Shoemaker, *Acta Crystallogr., Sect. B* **42,** 3 (1986).
4. Y. Andersson, *Acta Chem. Scand., Ser. A* **31,** 354 (1977).
5. H. F. Franzen and J. G. Smeggil, *Acta Crystallogr., Sect. B* **25,** 1736 (1969).
6. H. F. Franzen and J. G. Smeggil, *Acta Crystallogr., Sect. B* **26,** 125 (1970).
7. B. Harbrecht, *J. Less-Common Met.* **138,** 225 (1988).
8. H. Wada and M. Onoda, *Mater. Res. Bull.* **24,** 191 (1989).
9. S. J. Kim, K. S. Nanjundaswamy, and T. Hughbanks, *Inorg. Chem.* **30,** 159 (1991).
10. T. Degen and B. Harbrecht, *Acta Crystallogr., Sect. C* **51,** 2218 (1995).
11. B. Harbrecht, S. R. Schmidt, and H. F. Franzen, *J. Solid State Chem.* **53,** 113 (1984).
12. H. Nozaki, H. Wada, and S. Takekawa, *J. Phys. Soc. Jpn.* **60,** 3510 (1991).
13. B. Harbrecht and H. F. Franzen, *Z. Anorg. Allg. Chem.* **551,** 74 (1987).
14. M. Conrad, Thesis, Universitaet Dortmund, 1997.
15. M. Conrad and B. Harbrecht, *Z. Anorg. Allg. Chem.* **623,** 742 (1997).
16. B. Harbrecht, N. Rheindorf, and V. Wagner, *J. Alloys Compd.* **234,** 6 (1996).
17. B. Harbrecht and V. Wagner, *Z. Anorg. Allg. Chem.* **620,** 969 (1994).
18. J. V. Florio, R. E. Rundle, and A. I. Snow, *Acta Crystallogr.* **5,** 449 (1952).
19. F. Jellinek, *J. Less-Common Met.* **4,** 9 (1962).
20. E. Raub, H. Beeskow, and D. Menzel, *Z. Metallk.* **52,** 189 (1961).
21. V. Wagner and T. Degen, "DIFFRAKT: A Program for X-Ray Powder Diffraction," Universitaet Bonn, 1994.
22. G. M. Sheldrick, *Acta Crystallogr., Sect. A* **46,** 467 (1990).
23. G. M. Sheldrick, "SHELXL93: A Program for Crystal Structure Refinement," Universitaet Göttingen, 1993.
24. D. B. Wiles and R. A. Young, *J. Appl. Crystallogr.* **10,** 73 (1977).
25. A. J. Bradley and P. Jones, *J. Inst. Met.* **51,** 131 (1933).
26. S. Mahne and B. Harbrecht, *J. Alloys Compd.* **203,** 271 (1994).
27. B. G. Hyde and S. Andersson, *in* "Inorganic Crystal Structures," p. 342. Wiley, New York, 1988.
28. G. Perrault, *Can. Mineral.* **9,** 383 (1968).
29. H. Nyman, S. Andersson, B. G. Hyde, and M. O'Keeffe, *J. Solid State Chem.* **26,** 123 (1978).
30. Z. Bojarski and J. Leciejewicz, *Ach Hutn. Polska* **12,** 255 (1967); *Struct. Rep. A* **32,** 45 (1967).
31. H. Hirsch, A. Cugnac, M. Gadet, and J. Pouradier, *C. R. Acad. Sci., Ser. B* **263,** 1328 (1966).